Journal of Porous Materials (2022) 29:63–71
https://doi.org/10.1007/s10934-021-01141-w

Selective adsorption of CO_2/N_2 promoted by polar ligand functional groups of metal–organic frameworks

Wenxiu cao[1] · Bizhen Yuan[3] · Ou Zhuo[2] · Youji Li[2] · Wenhao Luo[4]

Accepted: 12 August 2021 / Published online: 29 August 2021
© The Author(s), under exclusive licence to Springer Science+Business Media, LLC, part of Springer Nature 2021

Abstract
The structure modification of metal–organic frameworks (MOFs) is a promising technique to enhance its selective adsorption of carbon dioxide at room temperatures. However, to date, little is known on the structure-property relationship of MOFs for carbon capture. In this work, the effects of chemical composition of MOFs on selective adsorption of carbon dioxide were studied systematically. A series of aluminum-based MIL-53 with similar formula units but different organic ligands, Al(OH)BDC-X [BDC = terephthalate, X = H, NH_2, NO_2, 2(CH_3)], were prepared and employed to the selective adsorption of CO_2/N_2. It was found that the Al(OH)BDC-X series with various organic ligands affected the CO_2 capacity significantly. The decorations of functional groups with strong polarity on the BDC links remarkably enhanced the CO_2 uptakes. The experimental results were in good agreement with the equivalent adsorption heat calculations, which showed that the CO_2 affinity of the ligands with polarity groups were thermodynamically more favored than those with non-polarity ones on the MOF structures. The interesting findings could provide a potential way to fabricate new metal organic frameworks with high carbon dioxide capture capacities at room temperature.

Keywords MIL-53(Al) · Polar functional groups · CO_2/N_2 selective adsorption · Equivalent adsorption heat

1 Introduction

Rising levels of atmospheric CO_2 from anthropogenic emissions have motivated the development of new technologies for CO_2 capture and conversion. Designing and developing materials for CO_2 capture is one of the grand challenges in the 21st century, among which the separation of CO_2 from N_2 in flue gas is particularly important [1–6]. At present, the state-of-the-art technology is to use alkanolamine aqueous solution to capture CO_2 from the post-combustion flue gas [7]. However, this process involves the formation of carbon-nitrogen bonds via the chemical interaction between amine functional groups and CO_2, causing the high cost for the regeneration of the adsorbent (the amine solution). Therefore, it is urgent to develop efficient materials and related processes for CO_2 capture that can effectively reduce the regeneration cost. Compared with amine-based absorption systems, physical sorbents is a more promising energy-efficient alternative. Therefore, great efforts have been devoted to developing physical sorbents for this purpose recently [8–14]. Still, limit material is capable of satisfying the criteria of 90% CO_2 capture at less than 35% increase in the cost of electricity, established by the Department of Energy (DOE)/National Energy Technology Laboratory (NETL) [15–17].

Several classes of materials, including ionic liquids (ILs), zeolites, porous carbons, porous organic polymers, covalent organic frameworks (COFs) and metal–organic frameworks

✉ Wenxiu cao
caowenxiu2007@126.com

Youji Li
bcclyj@163.com

1 Hunan Provincial Key Laboratory of Dark Tea and Jin-hua, College of Materials and Chemical Engineering, Hunan City University, Yiyang, People's Republic of China

2 Key Laboratory of Mineral Cleaner Production and Exploit of Green Functional Materials in Hunan Province, Jishou university, Jishou 416000, Hunan, People's Republic of China

3 College of Chemical Engineering and New Energy Materials, Zhuhai College of Jilin University, Zhuhai 519041, Guangdong, People's Republic of China

4 CAS Key Laboratory of Science and Technology on Applied Catalysis, Dalian Institute of Chemical Physics, Chinese Academy of Sciences, 457 Zhongshan Road, Dalian 116023, People's Republic of China

(MOFs), have been developed for CO_2 capture and conversion applications [18–28]. Particularly, MOFs have shown as a new class of crystalline porous materials with excellent performance in CO_2 capture, owing to their unique structural features and tunable physical and chemical properties. Especially, the functionalizable linkers, allowing for the incorporation of different capture sites, enable a fine-tuned properties of MOFs, making them promising materials for CO_2 capture. Enhancement of the interactions between the frameworks of MOFs and CO_2 has been developed as an efficient approach for CO_2 capture from CO_2/N_2 gas mixtures.

A large number of MOFs have been claimed as promising materials for CO_2 capture, but only a few MOFs have real industrial interests [29–32]. Compared with other MOFs, Aluminum-based MIL-53 stands out thanks to their high stability (for water, NO_x, SO_x, O_2), low-cost and nontoxic [31, 33, 34]. Another attractive aspect is that the adsorption and separation performance of CO_2/N_2 can be improved by introducing suitable functional groups [32, 35–37]. To understand the key factors that affect the CO_2 capture in essence, Study the adsorption mechanism of MOFs materials is needed. However, to date, such a systematic study on the effects of structural and surface properties of MOFs is scarce [38].

Here we attempt to disclose the correlation between the chemical composition of MOFs (e.g., organic linker) and the CO_2/N_2 selective adsorption. To achieve this, we chose a series of terephthalate-based MOFs (MIL-53 s) that had very close surface areas and chemical formula units. Four MIL-type MOFs, with similar formula unit (Al(OH)BDC-X, X = H, NH_2, NO_2, and 2(CH_3), BDC = terephthalate) were investigated to elucidate the influence of organic ligands on CO_2/N_2 selective adsorption. The CO_2 and N_2 adsorption isotherms of the Al(OH)BDC-X series materials were measured at 273 and 243 K. In comparing their CO_2 and N_2 uptake, correlations with their chemical compositions were discussed. Through this undertaking, the surface requirements of MOFs for a high CO_2/N_2 selective adsorption may be formulated, and such understanding will facilitate a more rational design of new MOF materials for CO_2/N_2 selective adsorption.

2 Experimental

The reagents used in materials preparation were commercially available and without further purification. These MOF materials were initially synthesized and activated according to the previous reports [35–37].

2.1 Synthesis of Al(OH)BDC -X [X = H, NO_2, NH_2, 2(CH_3)] materials

2.1.1 MIL-53(Al) (Al(OH)BDC-H)

The MIL-53(Al) material was synthesized hydrothermally under autogeneous pressure according to the reported procedures [35]. In a typical synthesis, the metal salt of $Al(NO_3)_3{\cdot}9H_2O$ was heated with terephthalic acid (H_2BDC) in H_2O with the molar ratio reported in the literature. The resultant solution was introduced into a teflon-lined stainless steel autoclave and then heated at 493 K for 72 h. The obtained MIL-53(Al) solids were dried overnight under vacuum at 573 K.

2.1.2 MIL-53(Al)-2CH_3 (Al(OH)BDC-2(CH_3))

The MIL-53(Al)-2(CH_3) material was synthesized hydrothermally under autogeneous pressure according to the reported procedures with slight changes [36]. In a typical synthesis, the metal salt of $AlCl_3{\cdot}6H_2O$ was heated with 2,5-dimethylterephthalic acid (BDC-2(CH_3)) in H_2O with the molar ratio reported in the literature. The resultant solution was introduced into a teflon-lined stainless steel autoclave and then heated at 483 K for 12 h. The obtained MIL-53(Al)-2CH_3 solids were dried overnight under vacuum at 423 K.

2.1.3 MIL-53(Al)-NH_2 (Al(OH)BDC-NH_2)

The MIL-53(Al)-NH_2 material was synthesized hydrothermally under autogeneous pressure according to the reported procedures [37]. In a typical synthesis, the metal salt of $Al(NO_3)_3$ was heated with 2-aminoterephthalic acid (HBDC-NH_2) in H_2O with the molar ratio reported in the literature. The resultant solution was introduced into a teflon-lined stainless steel autoclave and then heated at 403 K for 72 h. The obtained MIL-53(Al)-NH_2solids were dried overnight under vacuum at 423 K.

2.1.4 MIL-53(Al)-NO_2 (Al(OH)BDC-NO_2)

The MIL-53(Al)-NO_2 material was synthesized hydrothermally under autogeneous pressure according to the reported procedures [38]. In a typical synthesis, the metal salt of $Al(NO_3)_3{\cdot}9H_2O$ was heated with 2-nitroterephthalic acid (HBDC-NO_2) in H_2O with the molar ratio reported in the literature. The resultant solution was introduced into a teflon-lined stainless steel autoclave and then heated at 443 K for 12 h. The obtained MIL-53(Al)-NO_2 solids were dried overnight under vacuum at 423 K.

2.2 Characterization techniques

Powder X-ray diffraction (PXRD) patterns of the samples were obtained on a PW3040/60 X' Pert PRO (PANalytical) diffractometer using Cu Kα radiation (40 kV, 40 mA, λ = 0.15432 nm). IR spectra were recorded on an ATI Matheson Genesis in the spectral range 4000 – 400 cm^{-1} using the KBr disk method. Thermogravimetric (TG) analyses were carried out in air (75 mL/min, 35–800 °C, 4 °C/min) on a Netzsch STA-409CD. The BET surface area measurements were performed with N_2 adsorption/desorption isotherms at 77 K on a Belsorp-max instrument. The samples were outgassed under vacuum at 423 K for 24 h prior to measurements.

2.3 Gas adsorption measurements

Carbon dioxide and nitrogen adsorption isotherm at 273 and 243 K was measured using a static volumetric technique with an automatic adsorption apparatus (Belsorp-max, Japan). The sample holder was immersed in an ice water bath at 273 K (± 0.2 K) or ethanol water bath at 243 K(± 0.2 K). The 243 K constant temperature bath is made by mixing ethanol and water (70/30, v/v) in dewar flask and then cooling it to 243 K with liquid nitrogen. The good thermal insulation performance of dewar flask can keep the ethanol water bath at 243 K for 12 h. Typically, approximately 200 mg of sample was used for each gas adsorption measurement. Prior to the introduction of CO_2 or N_2 (99.99%), the samples were degassed in vacuum (at 10^{-4} torr) at 423 K for at least 12 h to remove any residual guest molecules in order to obtain the highest gas adsorption capacity.

2.4 Equivalent adsorption heat calculations

The equivalent adsorption heat of the Al(OH)BDC -X series materials was calculated by fitting the static adsorption isotherm and using Clausius-Claperyron equation. The equivalent adsorption heat (Q_{st}, kJ/mol) was calculated using the following equation (Eq. 1).

$$Q_{st} = \frac{RT_1T_2}{(T_2 - T_1)} \ln\left(\frac{p_2}{p_1}\right)_{n_a} \quad (1)$$

where p is the equilibrium adsorbate pressure (kPa), T is the adsorption temperature (K), R is the molar gas constant (8.314 J/(mol K)), and n_a is the adsorption capacity (cm^3/g).

3 Results and discussion

3.1 Characterization of Al(OH)BDC-X series materials

Powder XRD patterns for different Al(OH)BDC-X (X = H, NO_2, NH_2, $2(CH_3)$) materials are shown in Fig. 1. All the materials show a characteristic structure of the MIL-53(Al) [39, 41]. The diffraction peaks of Al(OH)BDC-X (X = H, NO_2, NH_2, $2(CH_3)$) materials were sharp and intense, indicating their highly crystalline nature. No impurity peaks were observed, confirming the high purity of the products.

The FT-IR spectra of the Al(OH)BDC-X (X=H, NO_2, NH_2, $2(CH_3)$) materials are shown in the Figs. S1–S4 (see supporting information). In the IR spectra of all the compounds, the strong absorption bands due to asymmetric and symmetric CO_2 stretching vibrations of the coordinated BDC-X linkers are located in the regions 1597–1616 cm^{-1} and 1415–1463 cm^{-1}, respectively [35]. The C–H stretching vibration of the -CH_3 group attached with the BDC-2CH_3 linker exhibits weak absorption bands at about 2970 and 2930 cm^{-1} in the IR spectra of Al(OH)BDC-2(CH_3) [36]. The broad signals between 3000 and 2500 cm^{-1} in the IR spectra of Al(OH)BDC-NH_2 are due to the aminoterephthalic acid in the pores [37].

To examine the thermal stability of all Al-MIL-53-X compounds, thermogravimetric analyses (TGA) were performed on all the compounds in air atmosphere. On the basis of the TG analyses, all the compounds are thermally stable up to 325–450 °C. In the TG curves of all the compounds (Supporting Information, Figs. S5–S8), any weight loss step

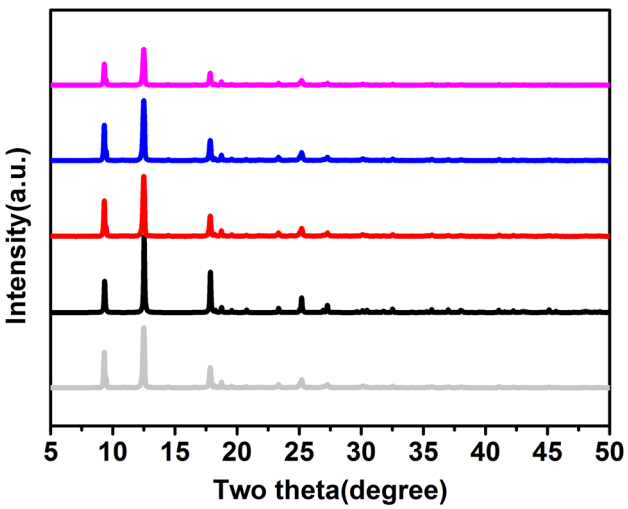

Fig. 1 PXRD patterns of Al(OH)BDC-X (X = H, NO_2, NH_2, $2(CH_3)$) series materials. MIL-53(simulated, gray), Al(OH)BDC-H (black), Al(OH)BDC-NH_2 (red), Al(OH)BDC-NO_2 (blue) and Al(OH)BDC-$2(CH_3)$ (magenta) (Color figure online)

that occurs below the decomposition temperature of the frameworks can be assigned to the removal of the occluded guest molecules (H_2O, H_2BDC-X linkers).

The specific surface areas of the Al(OH)BDC-X (X = H, NO_2, NH_2, 2(CH_3)) were determined by N_2 physisorption measurements at 77 K (Fig. 2). The isotherms are identified as type I, which is characteristic of micro-porous materials. The BET surface areas, Langmuir surface areas, pore size and micro-pore volume of the different samples are summarized in Table 1. Except Al(OH)BDC-2(CH_3), other Al(OH)BDC-X (X = H, NO_2, NH_2) showed similar N_2 isotherms with a similar BET surface area and micro-pore volume in the range of 850–1100 m^2/g and 0.31–0.38 cm^3/g. The BET surface area and micro-pore volume of the Al(OH)BDC-2(CH_3) was 741 m^2/g and 0.19 cm^3/g, which is slightly lower than the value obtained by Norbert Stock and coworkers on the material [36, 40].

Figure 3 is the pore size distributions of the Al(OH)BDC-X series materials calculated by the density functional theory (DFT) model, it shows that most of the pores fall into the size range of 0.6 to 0.8 nm. Among them, Al(OH)BDC-NO_2 and Al(OH)BDC-2(CH_3) have the smallest pore size, and the pore size of Al(OH)BDC-H (~0.8 nm) is coincident with the literature data [42–44].

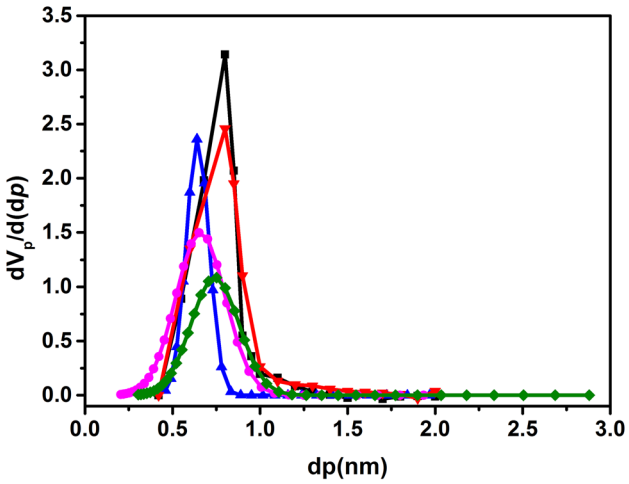

Fig. 3 The distribution of the pore size for Al(OH)BDC-X (X = H, NO_2, NH_2, 2(CH_3)). Al(OH)BDC-H (black, squares), Al(OH)BDC-NH_2 (red, down triangles), Al(OH)BDC-NO_2 (blue, up triangles) and Al(OH)BDC-2(CH_3) (magenta, circles) (Color figure online)

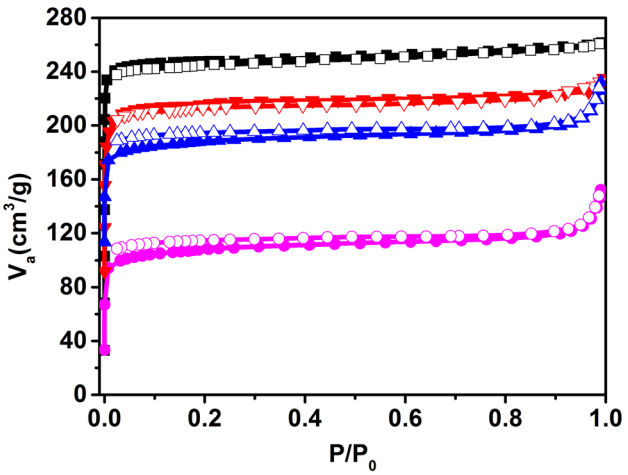

Fig. 2 Nitrogen adsorption (solid symbols) and desorption (empty symbols) isotherms for Al(OH)BDC-X (X = H, NO_2, NH_2, 2(CH_3)) measured at 77 K. Al(OH)BDC-H (black, squares), Al(OH)BDC-NH_2 (red, down triangles), Al(OH)BDC-NO_2 (blue, up triangles) and Al(OH)BDC-2(CH_3) (magenta, circles) (Color figure online)

3.2 Nitrogen and carbon dioxide isotherms

Figure 4 shows the nitrogen and carbon dioxide adsorption isotherms at 273 and 243 K for the Al(OH)BDC-X (X = H, NO_2, NH_2, 2(CH_3)) samples. The N_2 and CO_2 sorption properties of the Al(OH)BDC-X materials at 100 kPa are summarized in Table 2. It can be seen that the Al(OH)BDC-X series with various organic ligands affected the CO_2 and N_2 capacity significantly. Al(OH)BDC with functional groups can improve the adsorption capacity of N_2 and CO_2 simutaneously, with a more significant enhancement of CO_2 adsorption. It should be noted here that it seems ostensibly that the adsorption capacity of the Al(OH)BDC-2(CH_3) is lower than that of Al(OH)BDC-H, but the specific surface area and micro-pore volume of Al(OH)BDC-2(CH_3) synthesized in this paper are much lower than those of Al(OH)BDC-H, and

Table 1 BET and Langmuir surface areas, pore size and micro-pore volume for the Al(OH)BDC-X series materials

Al(OH)BDC-X	$S_{Langmuir}(m^2/g)^a$	$S_{BET}(m^2/g)^a$	Pore size(nm)	$V_{micro}(cm^3/g)^b$
H	1063	894	0.80	0.38
NO_2	847	698	0.65	0.31
NH_2	950	789	0.80	0.35
2(CH_3)	741	603	0.65	0.19

[a]Calculated over the relative pressure range $P/P_0 = 0.01–0.1$

[b]Pore volume at $P/P_0 = 0.1$

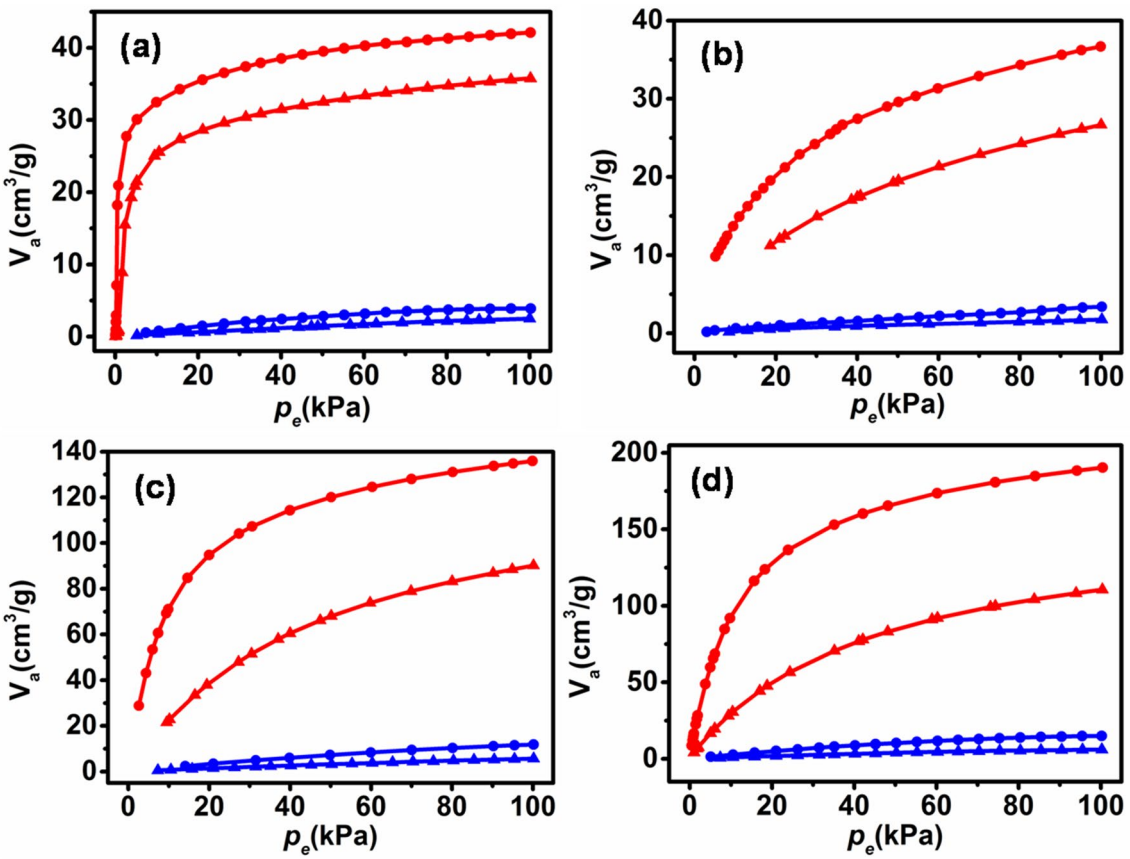

Fig. 4 The CO_2 (red) and N_2 (blue) adsorption isotherms of the Al(OH)BDC-X (X = H, NO_2, NH_2, $2(CH_3)$) series materials measured at 273 K (up triangles) and 243 K (circles), respectively. **a** Al(OH)BDC-H, **b** Al(OH)BDC $-2(CH_3)$, **c** Al(OH)BDC-NO_2, **d**Al(OH)BDC -NH_2 (Color figure online)

Table 2 CO_2 uptakes, N_2 uptakes and $R_{CO2/N2}$ of the Al(OH)BDC-X series materials at 273 and 243 K, and its isosteric heats of adsorption (Q_{st}) for N_2 and CO_2

	CO_2 uptake (cm^3/g)[a]		N_2 uptake (cm^3/g)[a]		$R_{CO2/N2}$[b]		Q_{st} (kJ/mol)	
Al(OH)BDC-X	273 K	243 K	273 K	243 K	273 K	243 K	N_2	CO_2
H	35.7	42.1	2.5	3.9	14.3	10.8	15–17	24–26
NO_2	90.1	135.9	5.6	11.8	16.1	11.5	17–18	30–32
NH_2	110	190	6	14.9	18.3	12.8	18–20	30–32
$2(CH_3)$	26.7	36.7	1.7	3.4	15.7	10.8	14–15	18–19

[a]At 100 kPa, [b]$R_{CO2/N2} = q_{CO2}/q_{N2}$

the micro-pore volume of the Al(OH)BDC-$2(CH_3)$ is even only half of the Al(OH)BDC-H, while the N_2 and CO_2 uptake of the Al(OH)BDC-$2(CH_3)$ is more than half of the Al(OH)BDC-H. Therefore, it proves that the introduction of CH_3 can improve the adsorption capacity of Al(OH)BDC-H for CO_2 and N_2. A similar conclusion was drawn in Zhong and co-works study, where the framework charges of the MOFs can effectively increase its adsorption capacity of CO_2 [45]. The high CO_2 adsorption capacity is attributed to the synergistic effect of pore structure and surface chemical properties of materials, and abundant micro-pores and nitrogen sites can significantly increase CO_2 adsorption capacity [46–48]. This is also confirmed by the adsorption-desorption experiment (Fig. S9) and repeated performance experiment (Fig. S10) of Al(OH)BDC-NH_2.

Table 2 showed the descending order of CO_2 uptake values at 100 kPa and 273 K is Al(OH)BDC-NH_2 (110 cm^3/g, 21.6 wt%) > Al(OH)BDC-NO_2 (90.1 cm^3/g, 17.7 wt%) > Al(OH)BDC-H (35.7 cm^3/g, 7.0 wt%) > Al(OH)BDC-$2(CH_3)$ (26.7 cm^3/g, 5.2 wt%). The CO_2 sorption capacities of the Al(OH)BDC-NH_2 is larger than the value of

the Kim and co-works (90 mg/g equal to 9 wt%) [49]. Except Al(OH)BDC-H and Al(OH)BDC-2(CH_3), the adsorption capacity of the Al(OH)BDC-X materials in this paper were higher than that of the Norbert group (4-NO_2 (10.8 wt%), 298 K) [36] and the Abid group (-NH_2 (75 cc/g), 273 K) [50]. The adsorption capacity of Al(OH)BDC-H is also lower than that of references [51–53] (6.58wt% at 303 K [51], 7.4 wt% at 288 K [52], 64 cm^3/g at 273 K [53]),and Al(OH)BDC-2(CH_3) is also lower than that of the Norbert group (6.8 wt% at 298 K) [36], which may be due to the fact that its micro-pore volume is half of that in the literature, because the linker of the Al(OH)BDC-2(CH_3) in this paper is 2,5-dimethyl-1,4-Benzenedicarboxylicacid, while 2-Methylterephthalic acid is used by the Norbert group.

The order of CO_2 adsorption capacity of Al(OH)BDC-X series materials at 100 kPa and 243 K is consistent with that at 273 K, Al(OH)BDC-NH_2 > Al(OH)BDC-NO_2 > Al(OH)BDC-H > Al(OH)BDC-2(CH_3). The adsorption capacity of CO_2 at low pressure (100 kPa) is closely related to the polarity of surface groups. The experimental results show that the materials modified by functional groups can improve their CO_2 adsorption capacity, and even the introduction of methyl with weak polar group can improve the CO_2 adsorption capacity of materials, which may be due to the fact that the introduction of methyl can enhance the interaction force between CO_2 and aromatic hydrocarbons, which is also confirmed by theoretical calculation [47]. Among them, Al(OH)BDC-NH_2 has the highest CO_2 adsorption capacity, which may be due to the strong dipole-quadrupole interaction between Al(OH)BDC-NH_2 and CO_2 molecules with high polarizability and fourth-order moment. Torrisi and Vaidhyanathanalso reported similar results that the nitrogen-containing materials can produce strong dipole-quadrupole interaction with CO_2 [41, 54].

In addition, the interaction between the functional group on the pore surface and CO_2 will also increase the selectivity of CO_2. It is an indisputable fact that functionalized MOFs can improve its selective adsorption performance for CO_2 [55, 56]. Table 3 shows the comparison of CO_2/N_2 selection factors of Al(OH)BDC-X series materials [49–51, 49–51]. The order of selective separation coefficient of CO_2/N_2 is that the separation coefficient of polar functional groups is higher than that of nonpolar or weakly polar ones, which is mainly because the polarity and fourth moment of CO_2 are higher than that of N_2, resulting in higher interaction force between CO_2 and material surface than that of N_2 [46, 59]. Table 3 also shows that the selectivity in this paper is similar to that in most literatures, but lower than that in the Abid group [50]. They used different co-solvents to synthesize a series of amine-MIL-53 materials, the separation factors of amine-MIL-53 series materials for CO_2/N_2 are quite different, which indicates that the solvent in the synthesis of the amino-MIL-53 material has a great influence on the CO_2/N_2 selectivity of the materials. In summary, introducing functional groups into MOF materials will enhance the CO_2/N_2 separation performance of the materials, especially the introduction of amino group.

Figure 5 show that the adsorption ratio of the Al(OH)BDC-X series material for CO_2 at 273 K is greater than that at 243 K. This is mainly due to the weakening of the interaction force between Al(OH)BDC-X and CO_2 at low temperature, which increases the influence of micro-pore volume and pore size on CO_2 adsorption capacity, and pore diameter has a greater influence on CO_2 adsorption capacity.

The Henry's law constants for CO_2 adsorption is shown in Table 4, The Henry's constant K_H in the Henry's law region was calculated by the standard procedures [60]. The Henry constant in Table 4 is expressed in three different

Table 3 Comparison of the selectivity among Al(OH)BDC-X series materials

Material	T(K)	P(atm)	Selectivity factor	References
MIL-53(Al)	303	1	8	[48]
Amino-MIL-53	303	1	18	[48]
MIL-53(Al)	350	5	7.5	[49]
Al(OH)BDC-H	243(273)	1	10(14.3)	This work
Al(OH)BDC-NO_2	243(273)	1	11.5(16.1)	
Al(OH)BDC-NH_2	243(273)	1	12.8(18.3)	
Al(OH)BDC-2(CH_3)	243(273)	1	10.8(15.7)	
MIL-53(Al)	298	1	10	[43]
MIL-53(Al)-NH_2	298	1	20	[43]
Amino-MIL-53	273	1	43	[44]
Amino-MIL-53-DMA(dimethylformamide and methanol/acetic acid)	273	1	43	[44]
Amino-MIL-53-DM(dimethylformamide and methanol)	273	1	153	[44]
Amino-MIL-53-DEA(dimethylformamide and ethanol/acetic acid)	273	1	637	[44]
Amino-MIL-53-DE(dimethylformamide and ethanol)	273	1	637	[44]

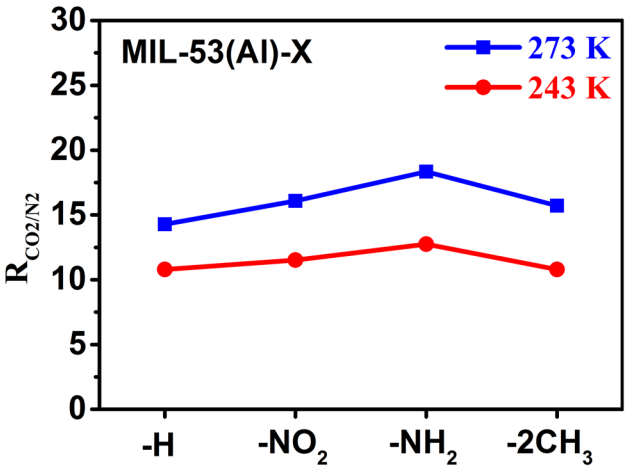

Fig. 5 The adsorption ratio of Al(OH)BDC-X (X = H, NO_2, NH_2, $2(CH_3)$) series materials for CO_2/N_2 adsorption (Color figure online)

Table 4 H's constant (K) of CO_2 for Al(OH)BDC-X series materials

	T(K)	H	NO_2	NH_2	$2(CH_3)$
K(mmol/(g atm))	273	0.9	11.4	17.7	4.8
	243	21.9	43.8	76.8	13.2
K(mmol/(g kPa))	273	0.01	0.11	0.18	0.05
	243	0.22	0.44	0.77	0.13
K(cm^3 /(g mmHg))	273	0.096	0.33	0.52	0.14
	243	0.64	1.28	2.25	0.39

units to facilitate comparison with previous experimental results. The Henry constant of CO_2 in this paper is larger than that of most Silica, Silicalite, MOF, ZIF and MIL in the room temperature range, but smaller than X-type zeolites [61, 62]. So compared with the literature, Al(OH)BDC-X series materials used in this paper have high Henry constant for CO_2, which also proves that these materials have strong interaction with CO_2 and are good CO_2 adsorbents.

3.3 The equivalent adsorption heat

The experimental equivalent adsorption heat of N_2 showed the following order in terms of appended functional groups (Fig. 6a): -NH_2 (18–20 kJ/mol) > -NO_2 (17–18 kJ/mol) > -H (15–17 kJ/mol) > -$2(CH_3)$ (14–15 kJ/mol). It is also showed that at zero coverage, Al(OH)BDC-X shows a high equivalent adsorption heat, and then drops sharply. The variation in N_2 sorption could potentially also arise from a difference in pore size distribution, with small pore sizes known to increase the adsorption capacity, as mentioned before. In particular, Al(OH)BDC-NO_2 has the highest zero adsorption heats, which may be due to its smallest pore diameter (0.65 Å). This extremely small pore size leads to stronger host guest interactions. In addition, it could be possible that NO_2-groups of adjacent linker molecules could interact with the gas molecules.

The experimental equivalent adsorption heat of CO_2 showed the following order in terms of appended functional groups (Fig. 6b): -NH_2 (30–32 kJ/mol) ≈ -NO_2 (30–32 kJ/mol) > -H (24–26 kJ/mol) > -$2(CH_3)$ (18–19 kJ/mol). It shows that with the increase of surface coverage, the adsorption heat of Al(OH)BDC-X series materials for CO_2 decreases sharply at first, and then tends to be flat. The adsorption heat by Al(OH)BDC-NH_2 is the highest in this series at zero coverage (ca. 57 kJ/mol). This is similar to the value of Kim's team (60 kJ/mol) [49], but higher than Abid's team (28 kJ/mol) [53]. The Q_{st} values of MIL-53(Al) obtained from the Sips and Toth models (Table 3) for CO_2 (25 kJ/mol) and N_2 (13 kJ/mol) are in agreement with previously published data [51, 62, 63]. It is noteworthy that

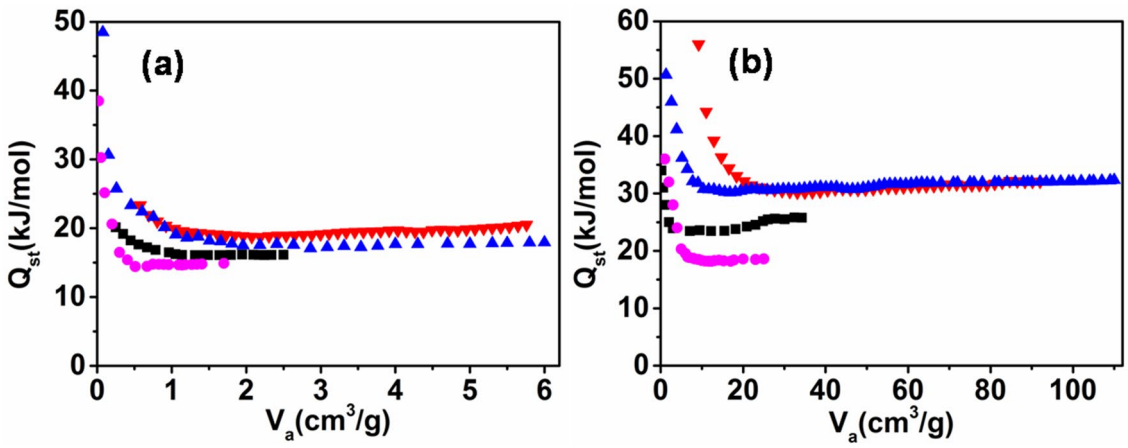

Fig. 6 **a** and **b** are the isosteric heats of N_2 and CO_2 of the Al(OH)BDC-X series materials, respectively. Al(OH)BDC-H (black), Al(OH)BDC-NH_2 (red), Al(OH)BDC-NO_2 (blue), and Al(OH)BDC-$2(CH_3)$ (magenta) (Color figure online)

the nitro and amine group functionalized network, show the highest adsorption heat for CO_2. The results show that the polar groups in the materials can effectively improve the adsorption heat of CO_2, increase the adsorption capacity of CO_2, and then effectively separate CO_2/N_2. This is consistent with the experimental and theoretical results in the literature [46, 59, 64].

In a word, the adsorption heat of Al(OH)BDC-X series materials for CO_2 is closely related to its functional group's polarity. The greater the polarity, the greater the adsorption heat, so it is very important to choose appropriate functional groups to improve the adsorption capacity of CO_2 and the selectivity of CO_2/N_2, which is similar to that reported in literature [59]. At the same time, their adsorption heat is between 25 and 35 kJ/mol, this medium adsorption heat is suitable for gas adsorption and separation application. This adsorption heat higher than that generated by physical adsorption (usually ~ 20 kJ/mol) is attributed to rich micropores and strong dipole-quadrupole interaction between CO_2 molecule and micro-porous polar framework.

4 Conclusions

The effects of organic ligand of MOFs on the selection adsorption of CO_2/N_2 of the materials have been elucidated. A series of MOFs, Al(OH)BDC with formula units but different organic linkers were prepared and employed as the receptors for carbon dioxide. It was found that the MOFs with different organic ligand affected the storage capacities of MOFs significantly. The decoration of functional groups with strong polarity on the organic linkers in MOFs could facilitate the adsorption of carbon dioxide on the ligands and thus enhance the carbon dioxide uptakes. The experimental results were in line with the equivalent adsorption heat calculations, which showed that the adsorption heat of the MOFs with polarity groups were much higher than those with non-polarity ones. Our findings could provide a potential way to fabricate new metal organic frameworks with high selective adsorption.

Supplementary Information The online version of this article contains supplementary material available (https://doi.org/10.1007/s10934-021-01141-w).

Acknowledgements This work was supported by the Educational Commission of Hunan Province (19B463), the Research Startup Foundation of Jishou University (No.21), and the Collaborative Innovation Center of Manganese-Zinc-Vanadium Industrial Technology (MXF202001).

Declarations

Conflict of interest The authors declare no conflict of interest.

References

1. Z. Zhang, Y. Zhao, Q. Gong, Z. Li, J. Li, Chem. Commun. **49**, 653 (2013)
2. Z. Shi, Y. Tao, J. Wu, C. Zhang, H. He, L. Long, Y. Lee, T. Li, Y.-B. Zhang, J. Am. Chem. Soc. **142**, 2750 (2020)
3. A. Kumar, D.G. Madden, M. Lusi, K.J. Chen, E.A. Daniels, T. Curtin, J.J. Perry, M.J. Zaworotko, Angew. Chem. Int. Ed. **54**, 14372 (2015)
4. I. Luz, M. Soukri, M. Lail, Chem. Sci. **9**, 4589 (2018)
5. H. Daglar, S. Keskin, J. Phys. Chem. C **122**, 17347 (2018)
6. Z. Li, G. Xu, B. Liu et al., Energies **8**, 11531 (2015)
7. G.T. Rochelle, Science **325**, 1652 (2009)
8. P. Murge, S. Dinda, S. Roy, Langmuir **35**, 14751 (2019)
9. A.M. Alloush, M.M. Abdelnaby, K.E. Cordova, N.A.A. Qasem, B.A. Al-maythalony, A. Jalilov, Y. Mankour, O. Hamouz, Micro. Meso. Mater. **305**, 110391 (2020)
10. Z. Yuan, M.R. Eden, R. Gani, Ind. Eng. Chem. Res. **55**, 3383 (2016)
11. J.M. Yu, L.H. Xie, J.R. Li, Y.G. Ma, J.M. Seminario, P.B. Balbuena, Chem. Rev. **117**, 9674 (2017)
12. J. Li, P.M. Bhatt, J. Li, M. Eddaoudi, Y. Liu, Adv. Mater. **32**, 2002563 (2020)
13. O.F. Altundal, C. Altintas, S. Keskin, J. Mater. Chem. A **8**, 14609 (2020)
14. J.R. Li, J. Sculley, H.C. Zhou, Chem. Rev. **112**, 869 (2012)
15. R.K. Pachauri, A. Reisinger, *IPCC Fourth Assessment Report* (Intergovernmental Panel on Climate Change, 2007)
16. S. Krachuamram, K. Chayakul, N. Kamonsutthipaijit, Micro. Meso. Mater. **310**, 110632 (2021)
17. K. Sumida, D.L. Rogow, J.A. Mason, T.M. McDonald, E.D. Bloch, Z.R. Herm, T.H. Bae, J.R. Long, Chem. Rev. **112**, 724 (2012)
18. B. Zheng, J. Bai, J. Duan, L. Wojtas, M.J. Zaworotko, J. Am. Chem. Soc. **133**, 748 (2011)
19. G. Sneddon, A. Greenaway, H.H.P. Yiu, Adv. Energ. Mater. **4**, 1301873 (2014)
20. J. Wang, S. Zhang, G. Cui, Chem. Soc. Rev. **45**, 4307 (2016)
21. Y. Li, L. Li, J. Yu, Chem. **3**, 928 (2017)
22. Y. Xie, T.T. Wang, X.H. Liu et al., Nat. Commun. **4**, 1960 (2013)
23. Z. Zhang, Y. Zhao, Q. Gong, Z. Li, J. Li. Chem. Commun. **49**, 653 (2013)
24. Z. Qiao, K. Zhang, J. Jiang, J. Mater. Chem. A **4**, 2105 (2016)
25. R. Vaidhyanathan, S.S. Iremonger, G.K.H. Shimizu, P.G. Boyd, S. Alavi, T.K. Woo, Science **330**, 650 (2010)
26. M.J. Lashaki, S. Khiavi, A. Sayari. Chem. Soc. Rev. **48**, 3320 (2019)
27. H.R. Abid, Z.H. Rada, X. Duan, H. Sun, S. Wang, Energ. Fuel **32**, 4502 (2017)
28. H. Yin, J. Wang, Z. Xie et al., Chem. Commun. **50**, 3699 (2014)
29. G. Singh, J. Lee, A. Karakoti, R. Bahadur, J. Yi, D. Zhao et al., Chem. Soc. Rev. **49**, 4360 (2020)
30. C.A. Trickett, A. Helal, B.A. Al-Maythalony, Z.H. Yamani, K.E. Cordova, O.M. Yaghi, Nat. Rev. Mater. **2**, 17045 (2017)
31. L. Liang, C. Liu, F. Jiang et al., Nat. Commun. **8**, 1233 (2017)
32. A.S. Munn, R.S. Pillai, S. Biswas et al., Dalton Trans. **45**, 4162 (2016)
33. A. Vimont, A. Travert, P. Bazin et al., Chem.Commun. **43**, 3291 (2007)
34. S. Vaesen, V. Guillerm, Q. Yang et al., Chem. Commun. **49**, 10082 (2013)
35. T. Loiseau, C. Serre, C. Huguenard, G. Fink, F. Taulelle, M. Henry, T. Bataille, G. Férey, Chem. Eur. J. **10**, 1373 (2004)
36. S. Biswas, T. Ahnfeldt, N. Stock, Inorg. Chem. **50**, 9518 (2011)

37. T. Ahnfeldt, D. Gunzelmann, T. Loiseau et al., Inorg. Chem. **48**, 3057 (2009)
38. X. Yan, T. Xue, Y. Liu et al., New Chem. Mater. **44**, 85 (2016)
39. C. Falaise, C. Volkringer, J. Facqueur et al., Chem. Commun. **49**, 10320 (2013)
40. W. Cao, Y. Li, L. Wang et al., J. Phys. Chem. C **115**, 13829 (2011)
41. A. Torrisi, R.G. Bell, C. Mellot-Draznieks, Micro. Meso. Mater. **168**, 225 (2013)
42. C. Serre, F. Millange, C. Thouvenot, M. Nogues, G. Marsolier, D. Louer, G. Ferey, J. Am. Chem. Soc. **124**, 13519 (2002)
43. T. Loiseau, C. Serre, C. Huguenard, G. Fink, F. Taulelle, M. Henry, T. Bataille, G. Ferey, Chem.-Eur. J. **10**, 1373 (2004)
44. W. Wang, L. Lin, H. Qi, W. Cao et al., Chin. J. Catal. **42**, 824 (2021)
45. C. Zheng, D. Liu, Q. Yang, C. Zhong, J. Mi, Ind. Eng. Chem. Res. **48**, 10479 (2009)
46. A. Torrisi, C. Mellot-Draznieks, R.G. Bell, J. Chem. Phys. **132**, 044705 (2010)
47. A. Torrisi, C. Mellot-Draznieks, R.G. Bell, J. Chem. Phys. **130**, 194703 (2009)
48. M.A. Hussain, Y. Soujanya, G.N. Sastry, J. Phys. Chem. C **119**, 23607 (2015)
49. J. Kim, W.Y. Kim, W.S. Ahn, Fuel **102**, 574 (2012)
50. H. Abid, Z.H. Rada, X. Duan et al., Energ. Fuel **32**, 4502 (2018)
51. B.C.R. Camacho, R.P.P.L. Ribeiro, I. A. A. C. Esteves. et al., Sep. Purif. Technol. **141**, 150 (2015)
52. S. Couck, J.F.M. Denayer, G.V. Baron et al., J. Am. Chem. Soc. **131**, 6326 (2009)
53. H.R. Abid, Z.H. Rada, J. Shang, S.B. Wang, Polyhedron **120**, 103 (2016)
54. R. Vaidhyanathan, S.S. Iremonger, G.K.H. Shimizu et al., Science **330**, 650 (2010)
55. P. Deria, S. Li, H. Zhang, R.Q. Snurr, J.T. Hupp, O.K. Farha, Chem. Commun. **51**, 12478 (2015)
56. J.R. Li, J. Yu, W. Lu, L.B. Sun, J. Sculley, P.B. Balbuena, H.C. Zhou, Nat. Commun. **4**, 1538 (2013)
57. S. Couck, E. Gobechiya, C.E.A. Kirschhock et al., ChemSusChem **5**, 740 (2012)
58. P. Mishra, H.P. Uppara, B. Mandal, S. Gumma, Ind. Eng. Chem. Res. **53**, 19747 (2014)
59. R. Dawson, D.J. Adams, A.I. Cooper, Chem. Sci. **2**, 1173 (2011)
60. S.A. Peter, J. Sebastian, R.V. Jasra, Ind. Eng. Chem. Res. **44**, 6856 (2005)
61. M. Pera-Titus, Chem. Rev. **114**, 1413 (2014)
62. P. Rallapalli, K.P. Prasanth, D. Patil, R.S. Somani, R.V. Jasra, H.C. Bajaj, J. Porous Mater. **18**, 205 (2011)
63. J. Möllmer, M. Lange, A. Möller, C. Patzschke, K. Stein, D. Lässig, J. Lincke, R. Gläser, H. Krautscheid, R. Staudt, J. Mater. Chem. **22**, 10274 (2012)
64. A. Torrisi, R.G. Bell, C. Mellot-Draznieks, Cryst. Growth Des. **10**, 2839 (2010)

Publisher's Note Springer Nature remains neutral with regard to jurisdictional claims in published maps and institutional affiliations.